

LETTER TO THE EDITOR

# An extremely prolific supernova factory in the buried nucleus of the starburst galaxy IC 694

M.A. Pérez-Torres<sup>1</sup>, C. Romero-Cañizales<sup>1</sup>, A. Alberdi<sup>1</sup>, and A. Polatidis<sup>2,3</sup>

<sup>1</sup> Instituto de Astrofísica de Andalucía - CSIC, 18008 Granada, Spain  
e-mail: torres@iaa.es

<sup>2</sup> Joint Institute for VLBI in Europe (JIVE), Dwingeloo, The Netherlands

<sup>3</sup> ASTRON, Dwingeloo, The Netherlands

Received MM DD, YYYY; accepted MM DD, YYYY

## ABSTRACT

**Context.** The central kiloparsec of many local Luminous Infra-red Galaxies are known to host intense bursts of massive star formation, leading to numerous explosions of core-collapse supernovae (CCSNe). However, the dust-enshrouded regions where those supernovae explode prevent their detection at optical and near-infrared wavelengths.

**Aims.** We investigate the nuclear region of the starburst galaxy IC 694 (=Arp 299-A) at radio wavelengths, aimed at discovering recently exploded CCSNe, to determine their rate of explosion, which carries crucial information on star formation rates, the initial mass function and starburst scenarios at work.

**Methods.** We use the electronic European VLBI Network to image with milliarcsecond resolution the 5.0 GHz compact radio emission of the inner 150 pc of IC 694

**Results.** Our observations reveal the presence of a rich cluster of 26 compact radio emitting sources in the central 150 pc of its nuclear starburst region. The large brightness temperatures observed for the compact sources indicate a non-thermal origin for the observed radio emission. Three of the newly discovered sources occurring in the eight months spanned by our observations are recently exploded core-collapse supernovae and, given their radio luminosities, correspond to a population of normal radio supernovae, likely arising from the explosion of Type IIb and Type IIL SNe. Our finding appears to rule out a starburst scenario with constant star formation in the nuclear region of IC 694, yields strong support for a recent (less than 10–15 Myr) instantaneous starburst, and suggests a top-heavy initial mass function for the stars in the innermost regions of IC 694. Even more important, our results challenge standard relations between observed far infrared luminosity and CCSN and star formation rates. Therefore, the application of those relationships to the high-redshift galaxies to estimate star formation and CCSN rates must be used with extreme care.

**Key words.** Galaxies: starbursts – luminosity function, mass function – individual: IC 694 – Stars: supernovae: general – Radiation mechanisms: non-thermal – Radio continuum: stars

## 1. Introduction

The observed rate at which massive stars ( $M \gtrsim 8 M_{\odot}$ ) die as CCSNe,  $\nu_{\text{CCSN}}$ , can be used as a direct measurement of the current star formation rate (SFR) in galaxies, and carries out precious information on the initial mass function (IMF) of massive stars. While the rate at which stars die in normal galaxies is rather small (e.g., one SN is expected to explode in the Milky Way every  $\sim 50$  yr), the CCSN rate in Luminous and Ultraluminous Infra-red Galaxies (LIRGs,  $L_{\text{IR}} \equiv L[8 - 1000 \mu\text{m}] \geq 10^{11} L_{\odot}$ ; and ULIRGs,  $L_{\text{IR}} \geq 10^{12} L_{\odot}$ ; Sanders & Mirabel (1996)) is expected to be at least one or two orders of magnitude larger than in normal galaxies (Condon 1992), and hence detections of SNe in (U)LIRGs offer a promising way of determining the current star formation rate in nearby galaxies.

However, the direct detection of CCSNe in the extreme densities of the central few hundred pc of (U)LIRGs is extremely difficult, as the optical and IR emission of supernovae is severely hampered by the huge amounts of dust present in those regions, and can at best yield an upper limit to the true value of  $\nu_{\text{CCSN}}$ . Fortunately, it is possible to directly probe the star forming activity in the innermost regions of (U)LIRGs by means of ultra-high angular resolution ( $\leq 0.05$  arcsec), ultra-high-sensitivity ( $\leq 0.05$

mJy) radio searches of CCSNe, as radio does not suffer from dust obscuration, and the angular resolution yielded by current Very Long Baseline Interferometry (VLBI) arrays, of the order of a few milliarcsec at cm-wavelengths, are able to detect individual radio supernovae at large distances in the local Universe.

Starburst activity in the circumnuclear regions of (U)LIRGs ensures both the presence of a high number of massive stars and a dense surrounding medium, so bright radio SNe are expected to occur (Chevalier 1982; Chugai 1997), and high-resolution radio observations have shown that highly-extinguished CCSNe do exist in the circumnuclear ( $r \lesssim 1$  kpc) region of local (U)LIRGs (Smith et al. 1998; Lonsdale et al. 2006; Colina et al. 2001; Neff et al. 2004; Pérez-Torres et al. 2007; Kankare et al. 2008). Therefore, VLBI observations can set strong constraints on the properties of star formation in the dust-enshrouded environments encountered in (U)LIRGs.

Arp 299 consists of two interacting galaxies (IC 694 and NGC 3690), which are in an early merger stage (Keel & Wu 1995). At a luminosity distance of 44.8 Mpc (Fixsen et al. 1996) for  $H_0 = 73 \text{ km s}^{-1} \text{ Mpc}^{-1}$ , Arp 299 has an infrared luminosity  $L_{\text{IR}} \approx 6.7 \times 10^{11} L_{\odot}$  (Sanders et al. 2003), which is nearly in the ULIRG category. The inner regions of Arp 299 (A, B, C and C' in Figure 1) are heavily dust-enshrouded regions, thus

making very difficult the optical and near-infrared detection of SNe. Yet, Arp 299 hosts recent and intense star forming activity, as indicated by the relatively high frequency of optically discovered supernovae in their outer, much less extinguished regions (Forti et al. 1993; van Buren et al. 1994; Li et al. 1998; Yamaoka et al. 1998; Qiu et al. 1999; Mattila et al. 2005).

The brightest component at infrared and radio wavelengths is IC 694 (A in the top panel of Figure 1; hereafter Arp 299-A), accounting for  $\sim 50\%$  of the total infrared luminosity of the system (Alonso-Herrero et al. 2000; Charmandaris et al. 2002), and for  $\sim 70\%$  of its 5 GHz radio emission (Neff et al. 2004). Numerous H II regions populate the system near star-forming regions, suggesting that star formation has been occurring at a high rate for the last  $\sim 10$  Myr (Alonso-Herrero et al. 2000). Given that IC 694 accounts for most of the infrared emission in Arp 299, it is the region that is most likely to reveal new SNe (Condon 1992). Since optical and near-infrared observations are likely to miss a significant fraction of CCSNe in the innermost regions of Arp 299-A due to huge extinctions [ $A_V \sim 34 - 40$  (Gallais et al. 2004; Alonso-Herrero et al. 2009)] and the lack of the necessary angular resolution, radio observations of Arp 299-A at ultra-high angular resolution, ultra-high sensitivity are the only way of detecting new CCSNe and measuring directly and independently of models its CCSN and star formation rates. In fact, Very Long Baseline Array (VLBA) observations carried out during 2002 and 2003 resulted in the detection of five compact sources (Neff et al. 2004), one of which (A0) was identified as a young SN.

## 2. eEVN observations and results

We used the electronic European VLBI Network (e-EVN) (Szomoru 2006) to image Arp 299-A at a frequency of 5 GHz, aimed at directly detecting recently exploded core-collapse supernovae through the variability of their compact radio emission. The attained off-source root-mean-square (r.m.s.) noise level was of  $39 \mu\text{Jy/beam}$  and  $24 \mu\text{Jy/beam}$  for the 8 April 2008 and 5 December 2008 observations, respectively, and reveal the existence of 15 and 26 compact components above 5 r.m.s. (see Figure 1).

Since the EVN radio image on 5 December 2008 is much deeper than the one obtained on 8 April 2008 (see appendix A for details), it is not surprising that we detected a larger number of VLBI sources in our second epoch. This allowed us to go back to our first-epoch image and extract the flux density for the new components (A15 through A25 in Figure 1), and which show  $\geq 5\text{r.m.s.}$  detections only in the December 2008 image). This procedure allowed us to recover four components above  $3\sigma$  (A15, A18, A22, and A25), based on a positional coincidence with the peak of brightness of our second epoch of better than  $\sim 0.5$  milliarcsec.

All of the 26 components but five (A0-A5) are reported for the first time, and demonstrate the existence of a very compact, rich, complex nuclear starburst in Arp 299-A. Indeed, the angular size encompassed by the radio emitting sources in Arp 299-A is less than  $0.7'' \times 0.4''$ , corresponding to a projected linear size of  $(150 \times 85)$  pc. To facilitate comparisons, we define here a fiducial supernova radio luminosity equal to three times the image r.m.s. in the 8 April 2008 epoch, which corresponds to  $2.9 \times 10^{26} \text{ erg s}^{-1} \text{ Hz}^{-1}$ . In this way, the radio luminosities for the VLBI components range between 1.1 (A25) and 7.3 (A1) and between 1.0 (A13) and 7.7 (A1) times the fiducial value, for the VLBI observations on 8 April 2008 and 5 December 2008, respectively (see Table 1 for details).

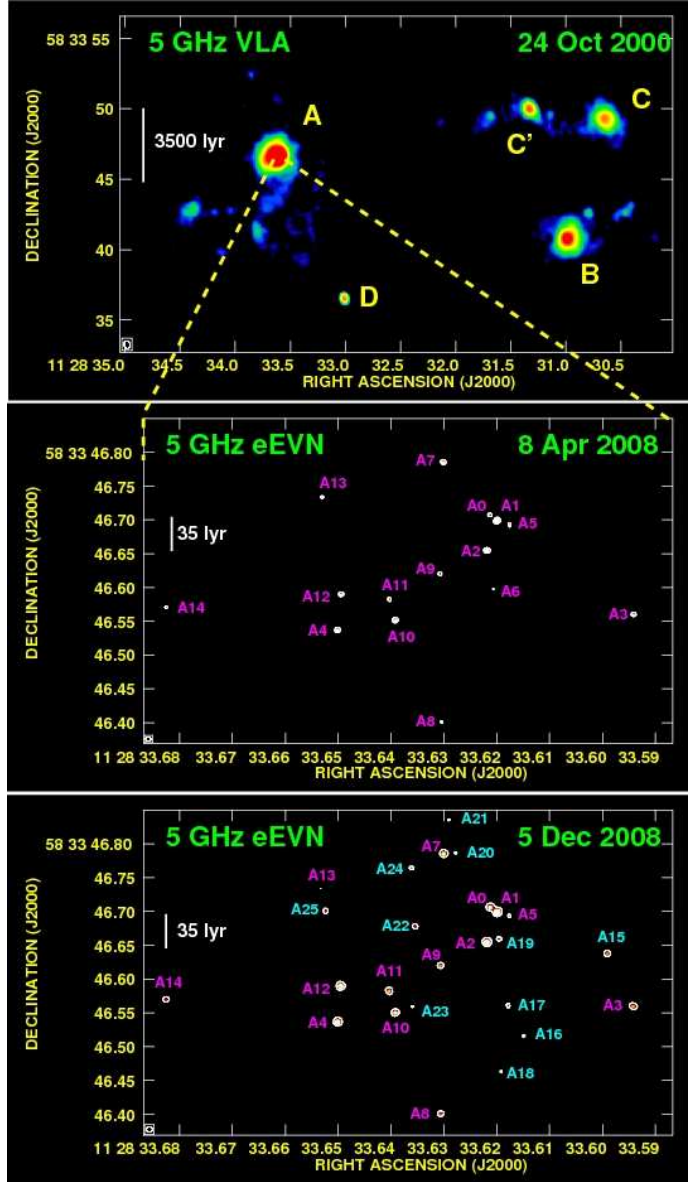


**Fig. 1.** *Top:* 5 GHz VLA archival observations of Arp 299 on 24 October 2000, displaying the five brightest knots of radio emission in this merging galaxy. *Middle and bottom:* 5 GHz eEVN observations of the central 500 light years of the Luminous Infrared galaxy Arp 299-A on 8 April 2008 and 5 December 2008, revealing a large population of relatively bright, compact, non-thermal emitting sources. The size of the FWHM synthesized interferometric beam was of  $(0.6 \text{ arcsec} \times 0.4 \text{ arcsec})$  for the VLA observations, and of  $(7.3 \text{ milliarcsec} \times 6.3 \text{ milliarcsec})$  and  $(8.6 \text{ milliarcsec} \times 8.4 \text{ milliarcsec})$  for the EVN observations on 8 April 2008 and 5 December 2008, respectively. To guide the reader's eye, we have shown in cyan the components detected only on the 5 December 2008 epoch.

## 3. Discussion

The radio emission from the compact sources detected from our VLBI observations can be explained in principle within two different physical scenarios: (i) thermal radio emission from super star clusters (SSCs) hosting large numbers of young, massive stars that ionize surrounding H II regions; (ii) non-thermal radio emission from supernova remnants (SNRs) and/or young radio

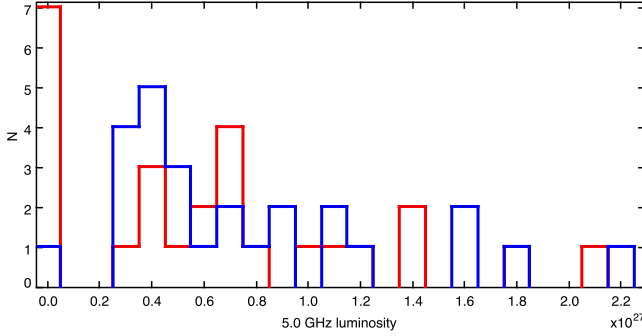


**Fig. 2.** 5.0 GHz luminosity histogram for the VLBI components detected on 8 April 2008 (red) and 5 December 2008 (blue). The values centered at 0.0 correspond to the upper limits quoted in Table 1. See main text for details.

supernovae (RSNe), i.e., recently exploded core-collapse supernovae where the interaction of their ejecta with their surrounding circumstellar or interstellar medium (CSM or ISM, respectively) would give rise to significant amounts of synchrotron radio emission.

The existence of SSCs in Arp 299-A has been demonstrated by their apparent detection using 2.2- $\mu\text{m}$  adaptive optics imaging (Lai et al. 1999). Further evidence in this direction comes from *Hubble Space Telescope* (HST) FOC and NICMOS images, which reveal a population of young stellar clusters in the central regions of Arp 299 (Alonso-Herrero et al. 2000). The total 5.0 GHz radio luminosity in compact sources is  $1.7 \times 10^{28} \text{ erg s}^{-1} \text{ Hz}^{-1}$  and  $2.0 \times 10^{28} \text{ erg s}^{-1} \text{ Hz}^{-1}$  on 8 April 2008 and 5 December 2008, respectively. However, the high flux densities in Table 1, coupled with the very low fitted angular sizes implied for most of the compact sources in Arp 299-A ( $\leq 9$  milliarcsec; see Table 2), indicate brightness temperatures,  $T_B$ , which largely exceed the thermal temperatures expected from SSCs ( $\lesssim 2 \times 10^4 \text{ K}$ ), thus ruling out a thermal origin for the compact radio emission traced by our eEVN observations.

Therefore, the observed radio emission must be due to young radio supernovae, SNRs, or both. We show in Table 1 the flux densities and luminosities for all the components identified in our observations, and classify the objects according to their variability. In particular, three sources (A6, A12, and A15) show significant flux density variations between our two consecutive VLBI observations (see Table 1 for details), which is very difficult to reconcile with their radio emission being due to SNRs. We conclude that the only plausible explanation is that the radio emission from those three compact sources is due to recently exploded CCSNe. A6 shows a decrease in flux density, while the flux densities of A12 and A15 rose between April and December 2008. Those variations are in good agreement with expectations from recently exploded CCSNe whose radio emission is either in its optically thin phase (A6), or still reaching its maxima at cm-wavelengths (A12 and A15).

The luminosities displayed by those RSNe range from  $\sim 4.0 \times 10^{26} \text{ erg s}^{-1} \text{ Hz}^{-1}$  (A15) to  $\sim 1.6 \times 10^{27} \text{ erg s}^{-1} \text{ Hz}^{-1}$  (A12), which are values typical of Type II plateau, or Type IIb SNe (Chevalier 2006). Those RSNe show a moderate, or even faint radio power, compared to their radio “loud” sisters, Type IIn SNe. To our knowledge, this is the first time that such a large population of “normal” radio SNe is found in the nuclear

starburst of a local (U)LIRG, unlike the case of ULIRG Arp 220, where essentially all discovered radio supernovae seem to be Type IIn, very powerful radio SNe (Parra et al. 2007). We note here that this is not simply a sensitivity issue, since some of the VLBI observations of Arp 220 had r.m.s. as low as  $9 \mu\text{Jy/b}$  (Parra et al. 2007), yet most of the objects detected there were identified, based on their large radio luminosities, as Type IIn SNe.

We also note that the positions for components A0 to A4 coincide with five VLBI components reported previously (Neff et al. 2004), while A5 through A14, and A15 through A26 were detected for the first time at 5.0 GHz on 8 April 2008 and on 5 December 2008, respectively. A0 through A4 still show significant radio emission, and A0 seems to be increasing its flux density at 5.0 GHz. One of those components, A0, was tentatively identified as a young SN (Neff et al. 2004). Given that A0 must have peaked at 5.0 GHz also in 2003 (Neff et al. 2004), this flux density increase may indicate that the SN is now interacting with a denser medium than previously encountered. At any rate, it is remarkable that A0 is still being detected six years after its peak, which indicates a rather low flux density decay –very unusual for standard radio supernovae– and suggests that A0 may be transitioning to a SNR phase. Components A1–A4 did not vary significantly their radio emission between our two observing epochs, so their radio emission is consisting with a SNR origin. We defer a detailed discussion of those sources to a future publication, since this is beyond the scope of this Letter and due to lack of space for a proper discussion.

If standard  $L_{\text{IR}}$  to  $\nu_{\text{CCSN}}$  relations and a Salpeter, or Scalo IMF are at work in Arp 299-A, implying  $\nu_{\text{CCSN}} \approx (2.7-3.7) \times 10^{-12} (L_{\text{IR}}/L_{\odot}) \text{ yr}^{-1}$ ; (Mattila & Meikle 2001; Condon 1992), Arp 299-A should show the death of massive stars at a rate of at most  $\sim (0.9-1.2) \text{ CCSN/yr}$ . However, our detection of at least three bright radio supernovae (A6, A12, and A15) in the central, dense  $\sim 150 \text{ pc}$  diameter nucleus of the luminous infra-red galaxy Arp 299-A in just eight months, appears to imply very unusual star-forming conditions in this galaxy, and is in conflict with standard  $L_{\text{IR}}$  to  $\nu_{\text{CCSN}}$  (and SFR) relations. Indeed, our observations imply a radio supernova rate of  $\approx 4 \text{ SN/yr}$ , which in turns would imply an infrared luminosity for Arp 299-A at least four times larger than is observed, since it is possible that faint radio emitting SNe are being missed.

Furthermore, our results argue strongly against starburst scenarios with a constant SFR in Arp 299-A, and yield strong support for a recent (less than 10–15 Myr) intense, instantaneous starburst (in agreement with previous results by Alonso-Herrero et al. (2000)) or, alternatively, a top-heavy IMF for the stars in Arp 299-A, in contrast with normally assumed Salpeter (Salpeter 1955), or Kroupa (Kroupa 2001) IMFs, where the production of massive stars ( $M \gtrsim 8 M_{\odot}$ ) that eventually result in CCSNe is low compared to the production of less massive stars. There seems to be evidence that this might also be the case of M 82 (Doane & Mathews 1993) and Arp 220 (Parra et al. 2007), and theoretically it is expected that in the warm dense ISM conditions within a (U)LIRG, the IMF should indeed be top-heavy due to a larger Jeans mass (Klessen et al. 2007). If this is true, it has important implications for the star-forming history of the Universe (van Dokkum 2008), because at higher redshifts a larger fraction of the star formation occurs in denser systems, causing a redshift dependence of the conversion factors between star formation indicators (including radio continuum) and the SFR.

*Acknowledgements.* We warmly thank L. Colina, A. Alonso-Herrero, J.M. Torrelles, E. Alfaro, and S. Mattila for many useful comments on the manuscript

**Table 1.** Compact radio emitting sources in the central region of Arp 299-A

Source Name <sup>d</sup>	Source Type	$\Delta \alpha^a$ (J2000.0)	$\Delta \delta$ (J2000.0)	$S_\nu$ ( $\mu\text{Jy}$ ) <sup>b</sup>		$L_\nu/10^{26}$ erg s <sup>-1</sup> Hz <sup>-1</sup>		$V^c$
				8 Apr 2008	5 Dec 2008	8 Apr 2008	5 Dec 2008	
A0	SN	33.6212	46.707	318±42	446±33	7.9±1.0	11.1±0.8	2.4
A1	SNR	33.6199	46.699	855±58	901±51	21.3±1.4	22.4±1.3	0.6
A2	SNR	33.6219	46.655	708±53	713±43	17.6±1.3	17.7±1.1	0.1
A3	SNR	33.5942	46.560	398±44	353±30	9.9±1.1	8.8±0.7	0.8
A4	SNR	33.6501	46.537	558±48	628±40	13.9±1.2	15.6±1.0	1.1
A5	SN?	33.6176	46.693	278±41	143±25	6.9±1.0	3.6±0.6	2.8
A6	SN	33.6206	46.597	208±40	≤72	5.2±1.0	≤1.8	3.4
A7	SNR	33.6300	46.786	496±46	468±34	12.3±1.2	11.6±0.8	0.5
A8	SNR	33.6306	46.401	226±41	264±27	5.6±1.0	6.6±0.7	0.8
A9	SNR	33.6306	46.620	294±42	282±28	7.3±1.0	7.0±0.7	0.2
A10	SNR	33.6392	46.551	550±48	436±32	13.7±1.2	10.9±0.8	2.0
A11	SNR	33.6403	46.583	300±42	351±30	7.5±1.0	8.7±0.7	1.0
A12	SN	33.6495	46.590	449±45	639±40	11.2±1.1	15.9±1.0	3.2
A13	SN?	33.6531	46.733	251±41	118±25	6.2±1.0	2.9±0.6	2.8
A14	SNR	33.6825	46.571	292±42	260±27	7.3±1.0	6.5±0.7	0.6
A15	SN	33.5991	46.638	159±40	304±28	4.0±1.0	7.6±0.7	3.0
A16	uncl.	33.6149	46.516	≤117	147±25	≤2.9	3.7±0.6	1.2
A17	uncl.	33.6179	46.561	≤117	179±26	≤2.9	4.5±0.6	2.4
A18	uncl.	33.6192	46.464	151±40	129±25	3.8±1.0	3.2±0.6	0.5
A19	SN?	33.6196	46.659	≤117	191±26	≤2.9	4.8±0.6	2.8
A20	uncl.	33.6278	46.789	≤117	146±25	≤2.9	3.6±0.6	1.2
A21	uncl.	33.6291	46.836	≤117	133±25	≤2.9	3.3±0.6	0.6
A22	uncl.	33.6354	46.678	173±40	217±26	4.3±1.0	5.4±0.7	0.9
A23	uncl.	33.6360	46.560	≤117	137±25	≤2.9	3.4±0.6	0.8
A24	uncl.	33.6361	46.764	≤117	166±25	≤2.9	4.1±0.6	2.0
A25	SN?	33.6524	46.701	132±40	209±26	3.3±1.0	5.2±0.7	1.6

<sup>a</sup> Coordinates are given with respect to  $\alpha(\text{J2000.0}) = 11:28:00.0000$  and  $\delta(\text{J2000.0}) = 58:33:00.000$ , and were obtained from the 5 December 2008 image. The positions for those sources also detected in 8 April 2008 coincide within the errors ( $\lesssim 0.5$  mas) with all of them.

<sup>b</sup> The uncertainty in the reported flux density for the detected compact components corresponds to  $1\sigma$ , where  $\sigma$  was determined by adding in quadrature the off-source r.m.s in each image and a 5% of the local maximum, to conservatively account for possible inaccuracies of the eEVN calibration.

<sup>c</sup> We define the significance of the flux density variability between the two consecutive epochs as  $V = |S_{\text{Dec}} - S_{\text{Apr}}| / \sqrt{\sigma_{\text{Dec}}^2 + \sigma_{\text{Apr}}^2}$ , where  $S_{\text{Apr}}$  and  $\sigma_{\text{Apr}}$  ( $S_{\text{Dec}}$  and  $\sigma_{\text{Dec}}$ ) are the values in columns 5 and 6 (7 and 8), respectively.

<sup>d</sup> Source names are given in right ascension order, except for the five components reported previously (A0 through A4) by (Neff et al. 2004).

and insightful discussions. The EVN is a joint facility of European, Chinese, South African and other radio astronomy institutes funded by their national research councils. MAPT, CRC, and AA acknowledge support by the Spanish Ministry of Education and Science (MEC) through grant AYA 2006-14986-C02-01. MAPT research is supported via a Ramón y Cajal Fellowship funded by the MEC and the Instituto de Astrofísica de Andalucía of the Spanish National Research Council (IAA-CSIC).

## References

Alonso-Herrero, A., Rieke, G. H., Colina, L., et al. 2009, *ApJ*, 697, 660  
Alonso-Herrero, A., Rieke, G. H., Rieke, M. J., & Scoville, N. Z. 2000, *ApJ*, 532, 845  
Charmandaris, V., Stacey, G. J., & Gull, G. 2002, *ApJ*, 571, 282  
Chevalier, R. A. 1982, *ApJ*, 259, 302  
Chevalier, R. A. 2006, *ArXiv Astrophysics e-prints*  
Chugai, N. N. 1997, *Ap&SS*, 252, 225  
Colina, L., Alberdi, A., Torrelles, J. M., Panagia, N., & Wilson, A. S. 2001, *ApJ*, 553, L19  
Condon, J. J. 1992, *ARA&A*, 30, 575  
Doane, J. S. & Mathews, W. G. 1993, *ApJ*, 419, 573  
Fixsen, D. J., Cheng, E. S., Gales, J. M., et al. 1996, *ApJ*, 473, 576  
Forti, G., Boattini, A., Tombelli, M., Herbst, W., & Vinton, G. 1993, *IAU Circ.*, 5719, 3  
Gallais, P., Charmandaris, V., Le Floch, E., et al. 2004, *A&A*, 414, 845  
Kankare, E., Mattila, S., Ryder, S., et al. 2008, *ApJ*, 689, L97  
Keel, W. C. & Wu, W. 1995, *AJ*, 110, 129  
Klessen, R. S., Spaans, M., & Jappsen, A.-K. 2007, *MNRAS*, 374, L29  
Kroupa, P. 2001, *MNRAS*, 322, 231  
Lai, O., Rouan, D., Rigaut, F., Doyon, R., & Lacombe, F. 1999, *A&A*, 351, 834

Li, W.-D., Li, C., Wan, Z., Filippenko, A. V., & Moran, E. C. 1998, *IAU Circ.*, 6830, 1  
Lonsdale, C. J., Diamond, P. J., Thrall, H., Smith, H. E., & Lonsdale, C. J. 2006, *ApJ*, 647, 185  
Mattila, S., Greimel, R., Gerardy, C., et al. 2005, *IAU Circ.*, 8477, 2  
Mattila, S. & Meikle, W. P. S. 2001, *MNRAS*, 324, 325  
Neff, S. G., Ulvestad, J. S., & Teng, S. H. 2004, *ApJ*, 611, 186  
Parra, R., Conway, J. E., Diamond, P. J., et al. 2007, *ApJ*, 659, 314  
Pérez-Torres, M. A., Mattila, S., Alberdi, A., et al. 2007, *ApJ*, 671, L21  
Qiu, Y. L., Qiao, Q. Y., Hu, J. Y., & Li, W.-D. 1999, *IAU Circ.*, 7088, 2  
Salpeter, E. E. 1955, *ApJ*, 121, 161  
Sanders, D. B., Mazzarella, J. M., Kim, D.-C., Surace, J. A., & Soifer, B. T. 2003, *AJ*, 126, 1607  
Sanders, D. B. & Mirabel, I. F. 1996, *ARA&A*, 34, 749  
Smith, H. E., Lonsdale, C. J., Lonsdale, C. J., & Diamond, P. J. 1998, *ApJ*, 493, L17  
Szomoru, A. 2006, in *Proceedings of the 8th European VLBI Network Symposium*  
van Buren, D., Jarrett, T., Terebey, S., et al. 1994, *IAU Circ.*, 5960, 2  
van Dokkum, P. G. 2008, *ApJ*, 674, 29  
Yamaoka, H., Kato, T., Filippenko, A. V., et al. 1998, *IAU Circ.*, 6859, 1

# Online Material

## Appendix A: eEVN observations of Arp 299-A

We observed the central regions of Arp 299-A at a frequency of 5 GHz in two epochs using the EVN. Our first epoch on 8-9 April 2008 (2008.99; experiment code RP009) included the following six antennas (acronym, diameter, location): Cambridge (CM, 32 m, United Kingdom), Medicina (MC, 32 m, Italy), Jodrell Bank (JB, 76 m, United Kingdom), Onsala (ON, 25 m, Sweden), Torun (TO, 32 m, Poland), and Westerbork array (WB, 25 m, The Netherlands). Our second observing epoch on 5 December 2008 (2008.340; RP014A experiment) included, in addition the EVN antennas Effelsberg (EF, 100 m, Germany), Knockin (KN, 25 m, United Kingdom), and Shanghai (SH, 25 m, China).

Both observing epochs consisted of e-VLBI phase-referenced experiments, using a data recording rate of 512 Mbps with two-bit sampling, for a total bandwidth of 64 MHz. The data were correlated at the EVN MkIV Data Processor at JIVE using an averaging time of 1 s. First epoch observations consisted of  $\sim 8.0$  hr on target. The telescope systems recorded both right-hand and left-hand circular polarization. 4.5 minute scans of our target source, Arp 299-A, were alternated with 2 minute scans of our phase reference source, J1128+5925. 3C345 and 4C39.25 were used as fringe finders and band-pass calibrators. Our second epoch consisted of  $\sim 4.5$  hr on target. The telescope systems also recorded in dual polarization, and 4.5 minute on-source scans were alternated with 1 minute scans of J1128+5925. The bright sources 3C84, 3C138, 4C39.25 and 3C286 were used as fringe finders and band-pass calibrators. (We note that the inclusion of EF in the second observing epoch allowed us to get a much better r.m.s., and this in spite of the significantly less amount of total observing time.)

We analyzed the correlated data for each epoch using the NRAO Astronomical Image Processing System (*AIPS*; <http://www.aips.nrao.edu>). The overall quality of the visibilities was good in both experiments. The performance of each antenna was checked by exporting the data of all amplitude and phase calibrators into the Caltech program DIFMAP. Within DIFMAP, we determined gain correction factors for CM, MC, JB, ON, TR and WB, respectively. After this procedure was completed within DIFMAP, the data were read back into AIPS for imaging purposes, using standard hybrid radio interferometric mapping techniques. Due to the limited bandwidth of CM and KN, the usable data of these antennas was found in a single sub-band with very noisy edges. To improve the quality of the bandpass calibration, we removed the edges of CM for the first epoch, and the edges of CM and KN for the second epoch. To obtain the maximum possible accuracy in the positions reported for the compact components in Figure 1, we first imaged the phase-reference source, J1128+5925, and then subtracted its contribution to the solutions of the delay and fringe rate for our target source, Arp 299-A, prior to obtaining the final eEVN images shown in Figure 1. We note, though, that this has no impact in the final images, since J1128+5925 is essentially point-like at the angular resolution ( $\lesssim 9$  milliarcseconds) provided by our 5 GHz e-EVN observations, and therefore its phase-contribution is negligible.

**Table 2.** Brightness temperatures<sup>a</sup> of the VLBI sources in Arp 299-A

Source		8 April 2008			5 December 2008			
Name	$S_\nu$ ( $\mu$ Jy)	$a$ (mas)	$b$ (mas)	$T_B$ (K)	$S_\nu$ ( $\mu$ Jy)	$a$ (mas)	$b$ (mas)	$T_B$ (K)
A0	318±42	≤ 2.8	...	...	446±33	5.3	3.0	$1.8 \times 10^6$
A1	855±58	≤ 3.6	...	...	901±51	2.1	1.8	$1.6 \times 10^7$
A2	708±53	≤ 2.5	≤ 1.5	$\geq 1.3 \times 10^7$	713±43	2.1	1.6	$1.4 \times 10^7$
A3	398±44	≤ 2.2	...	...	353±30	≤ 6.5	≤ 0.3	$\geq 1.2 \times 10^7$
A4	558±48	≤ 3.6	≤ 2.3	$\geq 1.0 \times 10^8$	628±40	≤ 2.8	≤ 0.5	$\geq 3.0 \times 10^7$
A5	278±41	≤ 11.1	≤ 1.2	$\geq 1.3 \times 10^6$	143±25	...	...	...
A6	208±40	≤ 7.6	≤ 1.4	$\geq 1.3 \times 10^6$	≤ 72	...	...	...
A7	496±46	≤ 2.5	≤ 3.3	$\geq 4.0 \times 10^6$	468±34	3.4	2.0	$4.6 \times 10^6$
A8	226±41	≤ 4.8	...	...	264±27	≤ 3.3	≤ 0.7	$\geq 7.6 \times 10^7$
A9	294±42	≤ 3.6	≤ 4.4	$\geq 1.2 \times 10^6$	282±28	...	...	...
A10	550±48	≤ 3.2	≤ 3.9	$\geq 2.9 \times 10^6$	436±32	...	...	...
A11	300±42	≤ 5.5	...	...	351±30	≤ 4.5	≤ 1.8	$\geq 2.0 \times 10^6$
A12	449±45	≤ 3.1	≤ 3.7	$\geq 2.6 \times 10^8$	639±40	2.3	1.5	$1.2 \times 10^7$
A13	251±41	≤ 3.3	≤ 4.2	$\geq 1.2 \times 10^6$	118±25	≤ 5.3	...	...
A14	292±42	≤ 5.0	≤ 3.7	$\geq 1.1 \times 10^6$	260±27	≤ 4.9	...	...
A15	159±40	...	...	...	304±28	≤ 2.8	≤ 1.6	$\geq 4.5 \times 10^6$
A16	≤ 117	...	...	...	147±25	5.6	3.2	$5.5 \times 10^5$
A17	≤ 117	...	...	...	179±26	7.3	3.9	$4.2 \times 10^5$
A18	151±40	...	...	...	129±25	≤ 5.1	≤ 5.5	$\geq 3.1 \times 10^5$
A19	≤ 117	...	...	...	191±26	≤ 4.0	≤ 2.0	$\geq 1.6 \times 10^6$
A20	≤ 117	...	...	...	146±25	≤ 7.9	≤ 3.5	$\geq 3.5 \times 10^5$
A21	≤ 117	...	...	...	133±25	≤ 7.4	≤ 2.9	$\geq 4.1 \times 10^5$
A22	173±40	...	...	...	217±26	≤ 8.6	≤ 4.3	$\geq 3.9 \times 10^5$
A23	≤ 117	...	...	...	137±25	≤ 8.8	≤ 2.9	$\geq 3.6 \times 10^5$
A24	≤ 117	...	...	...	166±25	≤ 8.6	≤ 7.0	$\geq 1.8 \times 10^5$
A25	132±40	...	...	...	209±26	≤ 8.6	≤ 4.4	$\geq 3.7 \times 10^5$

<sup>a</sup> The brightness temperatures shown for the 5.0 GHz VLBI source components in Arp 299-A were calculated using the flux densities in Table 1 and the angular sizes quoted here. We derived the brightness temperatures from the general formula:  $T_B = (2c^2/k) B_\nu \nu^{-2}$ , where  $B_\nu$  is the intensity, in  $\text{erg s}^{-1} \text{Hz}^{-1} \text{sr}^{-1}$ . Since  $B_\nu$  depends on the measured flux density,  $S_\nu$  and the angular sizes of the deconvolved angular size of each VLBI component (obtained by fitting them to elliptical Gaussians, characterized by their major and minor semi-axis,  $a$  and  $b$ ). Therefore, the above formula can be rewritten as  $T_B = (2c^2/k) B_\nu \nu^{-2} = 1.66 \times 10^9 S_\nu \nu^{-2} (ab)^{-1}$ , with  $S_\nu$  in mJy,  $\nu$  in GHz, and  $a$  and  $b$  in milliarcseconds, respectively.